

Causal posterior estimation

Simon Dirmeier* and Antonietta Mira^{†‡}

*Swiss Data Science Center, ETH Zurich, Switzerland

[†]Università della Svizzera italiana, Switzerland

[‡]Insubria University, Italy

Abstract

We present Causal Posterior Estimation (CPE), a novel method for Bayesian inference in simulator models, i.e., models where the evaluation of the likelihood function is intractable or too computationally expensive, but where one can simulate model outputs given parameter values. CPE utilizes a normalizing flow-based (NF) approximation to the posterior distribution which carefully incorporates the conditional dependence structure induced by the graphical representation of the model into the neural network. Thereby it is possible to improve the accuracy of the approximation. We introduce both discrete and continuous NF architectures for CPE and propose a constant-time sampling procedure for the continuous case which reduces the computational complexity of drawing samples to $\mathcal{O}(1)$ as for discrete NFs. We show, through an extensive experimental evaluation, that by incorporating the conditional dependencies induced by the graphical model directly into the neural network, rather than learning them from data, CPE is able to conduct highly accurate posterior inference either outperforming or matching the state of the art in the field.

1 Introduction

Consider the problem of inferring the Bayesian posterior distribution

$$\pi(\theta|x) \propto \pi(x|\theta)\pi(\theta) \quad (1)$$

when the evaluation of the likelihood function $\pi(x|\theta)$ is intractable, e.g., when its computation entails a high-dimensional integral, and only realizations from the joint distribution $\pi(x, \theta)$ can be generated. In machine learning, *simulation-based inference* (SBI) methods circumvent the need to evaluate the likelihood function and instead approximate the posterior distribution using a neural network trained on a synthetic data set of model outputs.

In particular, recent work has demonstrated that techniques from Bayesian inference based on neural density estimation with flow and score matching (Berner et al., 2024; R. T. Chen et al., 2018; Dirmeier & Perez-Cruz, 2023; Geffner & Domke, 2023; Lipman et al., 2023; Liu et al., 2023; Song et al., 2023; Vargas et al., 2022, 2023, 2024; Zhang & Chen, 2022) can be successfully adopted for SBI, enabling comparatively accurate posterior inference while scaling gracefully to high-dimensional parameter spaces (Gloeckler et al., 2024; Schmitt et al., 2024; Sharrock et al., 2024; Wildberger et al., 2023). For instance, the neural posterior method FMPE (Wildberger et al., 2023) approximates the posterior using a continuous normalizing flow (R. T. Chen et al., 2018; Lipman et al., 2023)

$$\pi(\theta|x) \approx q_1(\theta, x) = T_{\Lambda_1}[q_0(\cdot)](\theta) \quad (2)$$

where $q_0(\theta)$ is an arbitrary base distribution, such as a standard normal, $T_{\Lambda_1}[q_0(\cdot)](\theta)$ is a pushforward measure, i.e., a probability measure that is obtained from transferring a measure from one space to another, and where we denote with T_{Λ_1} the pushforward operator associated with the time-dependent diffeomorphism Λ_1 (which in Lipman et al. (2023) is called *flow*). The flow $\Lambda_t(\theta)$ induces a probability density path q_t , with $0 \leq t \leq 1$, starting at $q_0(\theta)$ and ending at an approximation to the posterior $\hat{\pi}(\theta|x) = q_1(\theta, x)$. If this flow is parameterized with a neural network that is sufficiently expressive and trained on an adequate amount of model outputs, i.e., realizations from the joint distribution $\pi(x, \theta)$, FMPE converges to the true posterior. In the same framework, neural SBI methods that approximate the posterior using ideas from denoising score matching (Geffner, Papamakarios, & Mnih, 2023; Gloeckler et al., 2024; Schmitt et al., 2024; Sharrock et al., 2024) have recently been introduced, impressively demonstrating both the accuracy and scalability of this framework.

Here, we propose a novel procedure for SBI that efficiently exploits the conditional dependence structure of the Bayesian model. Specifically, we design novel discrete and continuous normalizing flow (NF) architectures that incorporate the causal relationships of parameter and data nodes of the graphical models of the prior and posterior programs, which in *probabilistic programming* (van de Meent et al., 2018) refers to the graphical representation of the Bayesian model and its inversion, respectively, by hard-coding them into the neural network that parameterizes the flow. We demonstrate that the method, which we term *Causal Posterior Estimation*, (i) is more accurate than the state-of-the-art in multiple experimental benchmark tasks, (ii) has in general less trainable neural network weights if the number of parameters θ is in the order of around 10, and (iii) has empirically higher acceptance rates when drawing posterior samples. Additionally, we propose a constant-time $\mathcal{O}(1)$ sampling algorithm based on a rectified flow objective that matches the sampling efficiency of discrete normalizing flows. Interestingly, our method can be formalized within the framework of *structured semiseparable matrices*, making it computationally efficient on modern accelerators (Dao & Gu, 2024).

2 Preliminaries

In conventional Bayesian inference, the availability of a tractable likelihood function enables the use of Markov Chain Monte Carlo or variational inference methods (Blei et al., 2017; Brooks et al., 2011). In contrast, simulation-based inference (SBI) methods approximate the posterior distribution using a dataset of simulated outputs from the model. Specifically, neural SBI methods fit neural network-based approximations to the likelihood, posterior or likelihood-to-evidence ratio, using a synthetic data set of model outputs $\{(x_n, \theta_n)\}_{n=1}^N \sim \pi(x, \theta)$, where N is a simulation budget. Hence, while in the SBI framework we are not able to evaluate the likelihood, $\pi(x|\theta)$, we have access to a simulator function that allows drawing samples x_n . This is typically the case when $\pi(x|\theta)$ involves a high-dimensional integral over the latent variables of the model. In the following, we briefly introduce relevant methodology for later sections.

2.1 Gaussian flow matching and denoising score matching

Continuous normalizing flows (CNFs; R. T. Chen et al. (2018), Lipman et al. (2023), and Liu et al. (2023)) are neural network-based density estimators based on pushforward measures. The neural network is used to construct a time-dependent map $\Lambda_t(\theta)$, with $t \in [0, 1]$ defining

the ODE

$$\begin{aligned}\frac{d}{dt}\Lambda_t(\theta) &= v_{t_\phi}(\Lambda_t(\theta)) \\ \Lambda_0(\theta) &= \theta\end{aligned}\tag{3}$$

In Equation (3), $v_\phi : [0, 1] \times \mathbb{R}^{d_\theta} \rightarrow \mathbb{R}^{d_\theta}$ is a vector field that is modeled with a neural network with trainable weights ϕ , d_θ is the dimensionality of modeled variable and where we for convenience of notation drop the index ϕ in the following. In contrast to the discrete NF case (where v does not depend on time), v_t can be specified by any neural network without architectural constraints (e.g., it does not need to be invertible). Given an arbitrary base distribution $q_0(\theta)$, e.g., a standard normal, and a sample $\theta^{(0)} \sim q_0(\theta)$ solving the ODE in Equation (3) yields the pushforward

$$\begin{aligned}q_1(\theta) &= T_{\Lambda_1}[q_0(\cdot)](\theta) \\ &= q_0(\theta) \exp\left(-\int_0^1 \nabla v_t(\theta_t) dt\right)\end{aligned}\tag{4}$$

where ∇ is the divergence operator. The neural network parameters can be optimized by solving the maximum likelihood objective

$$\hat{\phi} = \arg \max_{\phi} \mathbb{E} [\log q_1(\theta)]\tag{5}$$

Since optimizing Equation (5) would require computing many network passes, training it is in practice often not feasible. Instead, Lipman et al. (2023) propose an alternative training objective which is computationally more favorable and which directly regresses v_t on a reference vector field u_t . The key insight of Lipman et al. (2023) is that, if the vector field u_t is chosen on a conditional basis, i.e., $u_t(\theta^{(t)}|\theta^{(1)})$, such that it induces a conditional probability density path $\varrho_t(\theta|\theta^{(1)})$, and such that

$$\begin{aligned}\varrho_0(\theta|\theta^{(1)}) &= \mathcal{N}(\theta; 0, I) \\ \varrho_1(\theta|\theta^{(1)}) &= \mathcal{N}(\theta; \theta^{(1)}, \sigma^2 I)\end{aligned}\tag{6}$$

then the training objective can be framed as a simple mean-squared error loss. Lipman et al. (2023) discuss several possibilities to define the probability paths ϱ_t and vector fields u_t and propose, amongst others, to use the ones that are defined by the optimal transport map

$$\begin{aligned}\varrho_t(\theta|\theta^{(1)}) &= \mathcal{N}(t\theta^{(1)}, (1 - (1 - \sigma_{\min})t)^2 I) \\ u_t(\theta|\theta^{(1)}) &= \frac{\theta_1 - (1 - \sigma_{\min})\theta}{1 - (1 - \sigma_{\min})\theta}\end{aligned}\tag{7}$$

where σ_{\min} is a hyperparameter (see the original publication for details). The *flow matching* training objective is then defined as

$$\hat{\phi} = \arg \min_{\phi} \mathbb{E}_{t \sim \mathcal{U}(0,1), \theta^{(1)} \sim \pi(\theta), \theta^{(t)} \sim \varrho(\theta^{(t)}|\theta^{(1)})} \|v_t(\theta^{(t)}) - u_t(\theta^{(t)}|\theta^{(1)})\|^2\tag{8}$$

Interestingly, Gaussian flow matching and denoising score matching belong mathematically to the same framework, but are defined via different forward processes (and reference vector

fields). Specifically, the variance-preserving SDE in the seminal paper by Song et al. (2021) can be recovered by setting

$$\begin{aligned} \varrho_t(\theta|\theta^{(1)}) &= \mathcal{N}\left(\alpha_{1-t}\theta^{(1)}, (1 - \alpha_{1-t}^2)I\right) \\ u_t(\theta|\theta^{(1)}) &= \frac{\alpha'_{1-t}}{1 - \alpha_{1-t}^2} \left(\alpha_{1-t}\theta - \theta^{(1)}\right) \end{aligned} \quad (9)$$

where α_t and α'_t are hyperparameters. In both cases, one can use the vector field v_t to sample deterministically or stochastically from the pushforward (Gao et al., 2025; Lipman et al., 2023; A. Tong et al., 2024).

2.2 Neural posterior estimation

SBI methods based on flow and denoising score matching (Gloeckler et al., 2024; Sharrock et al., 2024; Wildberger et al., 2023) that approximate the posterior distribution directly learn a vector field v_t by minimizing the least squares loss

$$\hat{\phi} = \arg \min_{\phi} \mathbb{E}_{t \sim \mathcal{U}(0,1), \theta^{(1)} \sim \pi(\theta), x \sim \pi(x|\theta^{(1)}), \theta^{(t)} \sim \varrho_t(\theta|\theta^{(1)})} \|v_t(\theta^{(t)}, x) - u_t(\theta^{(t)}|\theta^{(1)})\|^2 \quad (10)$$

Here, $v : [0, 1] \times \mathbb{R}^{d_\theta} \times \mathbb{R}^{d_x} \rightarrow \mathbb{R}^{d_\theta}$ is a function of time, data and a conditioning variable $x \in \mathbb{R}^{d_x}$. In comparison to the unconditional case (Equations (4) and (8)), this yields a conditional CNF $q_1(\theta, x)$ which can be used as an amortized posterior approximation $\hat{\pi}(\theta|x) = q_1(\theta, x)$.

After training, a sample from the posterior $\hat{\pi}(\theta|x_{\text{obs}})$ can be obtained by rejection sampling, i.e., by simulating $\theta^{(0)} \sim q_0(\theta)$ and solving the ODE in Equation (3) using off-the-self ODE solvers¹, such as Runge-Kutta methods, or with specialized solvers (Karras et al., 2022; Song et al., 2021). The simulated sample is accepted if it has non-zero density, i.e., if $\pi(\theta^{(1)}) \neq 0$, when evaluated under the prior.

3 Causal posterior estimation

We propose a new method for simulation-based inference that incorporates the conditional dependence (CD) structure of the Bayesian model in a novel normalizing flow architecture. To motivate the method, consider the factorization of the hierarchical model

$$\pi(\theta_1, \theta_2, \theta_3, x) = \pi(\theta_1)\pi(\theta_2|\theta_1)\pi(\theta_3)\pi(x|\theta_2, \theta_3) \quad (11)$$

which consists of four variables and a v -structure (see the graphical model in Figure 1), and assume that we are interested in inferring the posterior distribution

$$\pi(\theta_1, \theta_2, \theta_3|x) = \pi(\theta_1)\pi(\theta_2|\theta_1)\pi(\theta_3)\pi(x|\theta_2, \theta_3)/\pi(x) \quad (12)$$

Given the CD structure induced by the graphical model (Figure 1a), we argue that a neural network that only models the correlations $\rho(\theta_1, \theta_2|\theta_{\setminus 12})$, $\rho(\theta_2, x|\theta_{\setminus 2})$ and $\rho(\theta_3, x|\theta_{\setminus 3})$ and all CDs defined by the posterior program, i.e., the inverse of the graphical model (Figure 1b), should be equally expressive as a network that (implicitly) estimates all dependencies $\rho(\theta_1, \theta_2, \theta_3, x)$ (for instance, an attention-based transformer (Vaswani et al., 2017)).

¹For instance, as implemented in SciPy: https://docs.scipy.org/doc/scipy/reference/generated/scipy.integrate.solve_ivp.html

We consequently aim to construct a posterior estimator that explicitly incorporates the CD structure of both prior and posterior programs (Figure 1)².

In the following, we present the details of our method, Causal Posterior Estimation (CPE). We first present how we incorporate the prior program, then how the CD statements of the posterior program are accounted for, and finally show how the model is trained and can be sampled from. In this section, we introduce the continuous-time variant and only briefly describe the discrete NF architecture (see Appendix A for details on neural network architectures, the discrete NF variant, and other theoretical background).

3.1 Incorporation of the prior program

CPE approximates the true posterior $\pi(\theta|x)$ using a continuous normalizing flow (Equation (4)) which is parameterized by a neural network v_t . With the insight that for exponential family distributions the posterior mean is a convex combination of the prior mean and the likelihood (Diaconis & Ylvisaker, 1979), we design the vector field in Equation (4) as

$$v_t(\theta, x) = \gamma\theta + (1 - \gamma)\lambda_t(\theta, x) \quad (13)$$

where $\gamma \in [0, 1]$ is a trainable parameter and λ_t is a time-dependent map that is parameterized by a neural network. The field v_t is naturally invertible iff λ_t is invertible (which is a necessary condition in the discrete NF case, but uncritical in the continuous NF case). To incorporate the prior program in the flow, we simply choose, as a base distribution, the prior, i.e., $q_0(\theta) := \pi(\theta)$. While it might seem unnecessary to account for both posterior and prior programs, recent work has shown that the accuracy in Bayesian inferential problems can be improved if the forward pass of the prior program is incorporated (Ambrogioni et al., 2021). Constructing the push-forward as a convex combination with initial inputs $\theta \sim \pi(\theta)$ for sampling has, whilst being straight-forward and intuitive, curiously not been described before in the SBI literature.

3.2 Incorporation of conditional dependencies

The pushforward is parameterized by a map λ_t which we will describe in the following.

Causal factorization Assume that the posterior program of the model has the structure of a directed acyclic graph³. We sort the parameter nodes of the posterior program in

²There are several approaches to invert a graphical model (Stuhlmüller et al., 2013; Webb et al., 2018). Here, we adopt the approach by Ambrogioni et al. (2021) for its simplicity. The method by Webb et al. (2018), whilst preferable, yields denser inverses and we did not observe performance improvements in preliminary experiments.

³This assumption is not restrictive, since even generative models with loops, such as dynamic Bayesian networks, can be unrolled such that the generative model is acyclic. Also, cyclic generative models are only very rarely (if ever) used in probabilistic inference.

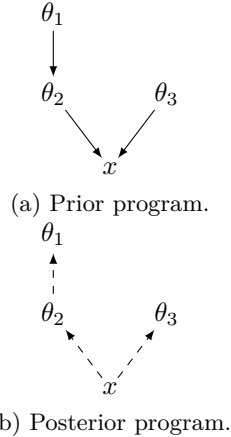


Figure 1: Graphical model of Equation (11).

topological order. For instance, in the graphical model in Figure 1b, a possible topological ordering is given by $\omega = \{3, 2, 1\}$. We then sort the variables based on their topological ordering and construct a mapping λ_t that models

$$p(x, \theta) = p(x) \prod_i^{d_\theta} p(\theta_{\omega_i} | \theta_{<\omega_i}, x) \quad (14)$$

Specifically, we model each factor of Equation (14) using a neural network f_i , i.e., $\theta'_{\omega_i} = f_i(\theta_{\leq \omega_i})$, in such a way that the conditional dependencies of the posterior model, and only those, are retained when transforming $\theta_{\leq \omega_i}$ to θ'_{ω_i} . One way to do this, is to design a lower-triangular matrix $W \in \mathbb{R}^{d_\theta \times d_\theta}$ and, ordering the nodes of the DAG topologically, setting all $W_{i < j} = 0$, i.e.,

$$W = \begin{bmatrix} g(W_{1,1}) & 0 & \cdots & 0 \\ W_{2,1} & g(W_{2,2}) & \cdots & 0 \\ \vdots & \vdots & \ddots & \vdots \\ W_{d_\theta,1} & W_{d_\theta,2} & \cdots & g(W_{d_\theta,d_\theta}) \end{bmatrix} \quad (15)$$

where $g : \mathbb{R} \rightarrow \mathbb{R}$ is a random element-wise activation function that can also be the identity function (see Section 3.4). To avoid needlessly modeling additional conditional dependencies, we set all matrix elements $W_{ij} = 0$ where

$$\theta_i \perp\!\!\!\perp \theta_j \mid \theta_{\setminus ij}, x \quad (16)$$

in the posterior program. For instance, for the posterior program in Figure 1b we define the linear transform for the topological ordering $\omega = \{3, 2, 1\}$

$$W = \begin{bmatrix} g(W_{1,1}) & 0 & 0 \\ 0 & g(W_{2,2}) & 0 \\ 0 & W_{2,3} & g(W_{3,3}) \end{bmatrix} \quad (17)$$

Block matrix projection Furthermore, instead of using W as a projection, we additionally augment the transformation with auxiliary dimensions forming a block-matrix B where for each variable θ_i we use a block of size $d_{\text{in}} \times d_{\text{out}}$ with $d_{\text{in}}, d_{\text{out}} \geq 1$. Augmenting projections with auxiliary variables has previously been reported to increase expressivity of normalizing flow models (Ambrogioni et al., 2021; Cornish et al., 2020; Dupont et al., 2019). The attentive reader might have noticed that parameterizing all f_i jointly using a transform B is a form of a *block neural autoregressive flow* (De Cao et al., 2020; C.-W. Huang et al., 2018). To construct a map $f : \mathbb{R}^{d_\theta} \rightarrow \mathbb{R}^{d_\theta}$, we stack several block matrices and construct a sequence of transformations $f = (f^{(1)}, \dots, f^{(K)})$ where each $f^{(k)}$ is a linear projection

$$f^{(k)}(\theta) = \text{act} \left(B^{(k)}(\theta) + b^{(k)} \right) \quad (18)$$

$b^{(k)} \in \mathbb{R}^{d_{\text{out}}^{(k)} d_\theta}$ is an offset term, act is an arbitrary activation function, and the block sizes are set to $d_{\text{in}}^{(1)} = d_{\text{out}}^{(K)} = 1$ and the rest are user-defined integers.

If B is sufficiently sparse, it belongs to the family of *structured semiseparable matrices* which can be represented with sub-quadratic parameters and which have fast matrix multiplication operations (Dao & Gu, 2024; Fu et al., 2023; Katharopoulos et al., 2020). As a consequence, the block matrices can be computed efficiently on modern computing hardware without masking procedures. While we did not implement the algorithms introduced in,

e.g., Dao and Gu (2024), here, modeling B as semiseparable matrix opens up efficient implementation possibilities for our model. For posterior programs with non-sparse structure, the blocks in B can be modeled to enforce a low-rank structure via defining each block

$$B_{ij} = \xi_{ij}\zeta_{ij}^T \quad (19)$$

where ξ_{ij}, ζ_{ij} are trainable vectors.

Conditioning on time and data To condition the flow on continuous time variables t and data x , we first compute random Fourier features for t (Song et al., 2021; Tancik et al., 2020). We then project the Fourier features and data through two independent MLPs before concatenating the projections and using them as conditioning vectors. In this work, we add the conditioning vectors to the leaf nodes of the posterior program after the first flow layer $f^{(1)}$ (as is typically done in autoregressive flows (Germain et al., 2015; Kingma et al., 2016; Papamakarios et al., 2017)), even though conditioning after each layer is naturally possible (see Appendix A for details).

3.3 Training and constant time sampling

Sampling from $q_1(\theta, x)$ can be performed using a conventional ODE solver requiring $\mathcal{O}(T)$ steps. By training the flow to find a straight transport map from the base distribution q_0 (i.e, the prior distribution; see Section 3.1) to the posterior $q_1(\theta, x)$, sampling can be performed with constant time complexity $\mathcal{O}(1)$. Specifically, we train CPE using the *rectified flow* objective (Liu et al., 2023)

$$\hat{\phi} = \arg \min_{\phi} \mathbb{E}_{t, \theta^{(1)}, x, \theta^{(0)}} \left[\|\theta^{(1)} - \theta^{(0)} - v_t(\theta^{(t)}, x)\|^2 \right], \quad \text{with } \theta^{(t)} = t\theta^{(1)} + (1-t)\theta^{(0)} \quad (20)$$

We can then draw a posterior sample $\theta^{(1)} \sim q_1$ by solving Equation (4). Starting from a prior draw $\theta^{(0)} \sim \pi(\theta)$ and a fixed discretization steps $dt = \frac{1}{20}$, we solve the ODE using an Euler solver where we use a small constant value of $T = 20$ steps to account for approximation errors in the learned transport map.

3.4 Discrete vs continuous pushforwards

The time-dependent map v_t is not required to have any architectural constraints, since sampling using an ODE is trivially invertible. However, we can define a discrete normalizing flow architecture by dropping the argument t and defining $v : \mathbb{R}^{d_\theta} \times \mathbb{R}^{d_x} \rightarrow \mathbb{R}^{d_\theta}$. The forward transform defined in Equation (18) is invertible given x if g is invertible and strictly positive, and the activation functions are invertible (see Appendix A for details). While the inverse $v^{-1}(\cdot, x)$, which is required for sampling, does not have an analytical solution, it can be easily found by, e.g., bifurcation or by training a regressor neural network on pairs of posterior and prior samples $(\theta^{(1)}, \theta^{(0)})$.

3.5 Amortized vs sequential inference

Sequential SBI procedures have been shown to be able to improve the accuracy of the posterior approximation $\pi(\theta|x_{\text{obs}})$ when the goal is to estimate the posterior for a single observation, x_{obs} , rather than obtaining an amortized solution (Deistler et al., 2022; Durkan et al., 2020; Greenberg et al., 2019; Gutmann, Cor, et al., 2016; Hermans et al., 2020; Lueckmann et al., 2017; Miller et al., 2022; Papamakarios & Murray, 2016; Papamakarios et al., 2019; Sharrock et al., 2024). CPE can be readily adopted to the truncation approach

by Sharrock et al. (2024) to allow for sequential inference (even though we leave this for future work here).

4 Related work

Flow and denoising score matching Flow and denoising score matching approaches have recently been applied with great success in applications ranging from generative modeling (Albergo & Vanden-Eijnden, 2023; De Bortoli et al., 2021; Ho et al., 2020; Karras et al., 2022; Lipman et al., 2023; Liu et al., 2023; Song & Ermon, 2019; Song et al., 2021; A. Y. Tong et al., 2024), to Bayesian (variational) inference (Berner et al., 2024; Dirmeier & Perez-Cruz, 2023; Geffner & Domke, 2023; Lipman et al., 2023; Liu et al., 2023; Vargas et al., 2022, 2023, 2024; Zhang & Chen, 2022), to inverse problems (Chung et al., 2022, 2023; Dou & Song, 2024; Kadkhodaie & Simoncelli, 2021; Kavar et al., 2021, 2022; Rout et al., 2023).

Simulation-based inference In neural SBI, multiple methods based on flow and denoising score matching have been proposed. While several methods (Deistler et al., 2022; Greenberg et al., 2019; Lueckmann et al., 2017; Papamakarios & Murray, 2016; Radev et al., 2023) suggested applying mixture density networks or discrete normalizing flows for inferring posterior distributions, Geffner, Papamakarios, and Mnih (2023), Gloeckler et al. (2024), Schmitt et al. (2024), Sharrock et al. (2024), and Wildberger et al. (2023) proposed continuous-time alternatives where training objectives either utilize flow matching or score matching losses (Gao et al., 2025; A. Tong et al., 2024). Most related to our work, Gloeckler et al. (2024) employ a transformer-based neural network which allows to encode the correlation structure of the posterior. In comparison to our work, their work is based on simple masking mechanisms that define the correlations of the posterior program and which need to be refined which each transformer layer. Our method does not have this requirement and directly incorporates the conditional dependencies in the neural network. Also, their approach only considers the posterior program while our work models both prior and posterior conditional dependencies. Furthermore, we introduce an architecture which can be inverted in case a discrete normalizing flow should be utilized while their neural network is not invertible.

Instead of approximating the posterior directly, other approaches aim to find neural approximations to the likelihood (Dirmeier, Albert, & Perez-Cruz, 2023; Glöckler et al., 2022; Pacchiardi & Dutta, 2022; Papamakarios et al., 2019) or the likelihood-to-evidence ratio (Delaunoy et al., 2022; Hermans et al., 2020; Miller et al., 2022). Furthermore, for high-dimensional problems, it can often be advantageous to compute a collection of near-sufficient summary statistics (Albert et al., 2022; Y. Chen et al., 2021, 2023) and then apply either neural SBI or ABC methods (Albert et al., 2015; Beaumont et al., 2009; Del Moral et al., 2012; Sisson et al., 2018).

An important but unrelated line of research focuses on *robust* SBI methods (Delaunoy et al., 2022; Dellaporta et al., 2022; Frazier et al., 2020; Gloeckler et al., 2023; Hermans et al., 2022; D. Huang et al., 2023; Kelly et al., 2024; Verma et al., 2025; Ward et al., 2022; Yuyan et al., 2025), i.e., methods that can account for model misspecification and poor calibration. The contributions of this work are orthogonal to this research and we expect that CPE, similarly to other NPE methods, only poorly handles misspecification necessitating future work in this direction.

5 Experiments

We evaluate CPE in an experimental setting using nine SBI benchmark tasks. We compare CPE against the state-of-the-art baselines Flow Matching Posterior Estimation (FMPE; Wildberger et al. (2023)), Posterior Score Estimation (PSE; Sharrock et al. (2024)) and All-in-One Posterior Estimation (AIO; Gloeckler et al. (2024)) to demonstrate the competitiveness of our method.

For each benchmark task we simulate five different synthetic data sets, each consisting of a random observable and parameter sampled from the generative model $(x_{\text{obs}}, \theta) \sim \pi(x, \theta)$, and then attempt to infer an accurate approximation to the posterior $\hat{\pi}(\theta|x_{\text{obs}})$ (Appendix B for details on experimental models). We compare the approximation to a "ground-truth" posterior which we infer using a Markov Chain Monte Carlo sampler, meaning that here all benchmark tasks have a tractable likelihood function while this is not the case in real-world applications (Appendix C for details). We compare the inferred posteriors to the ground-truth posteriors using the H-min divergence (Dirmeier, Albert, & Perez-Cruz, 2023; Zhao et al., 2022) and classifier-two-sample-tests (C2ST; Lopez-Paz and Oquab (2017)) using different data set sizes. All methods use a Runge-Kutta 5(4) solver and we additionally use an Euler solver with $T = 20$ steps for CPE. CPE convincingly outperforms or matches the

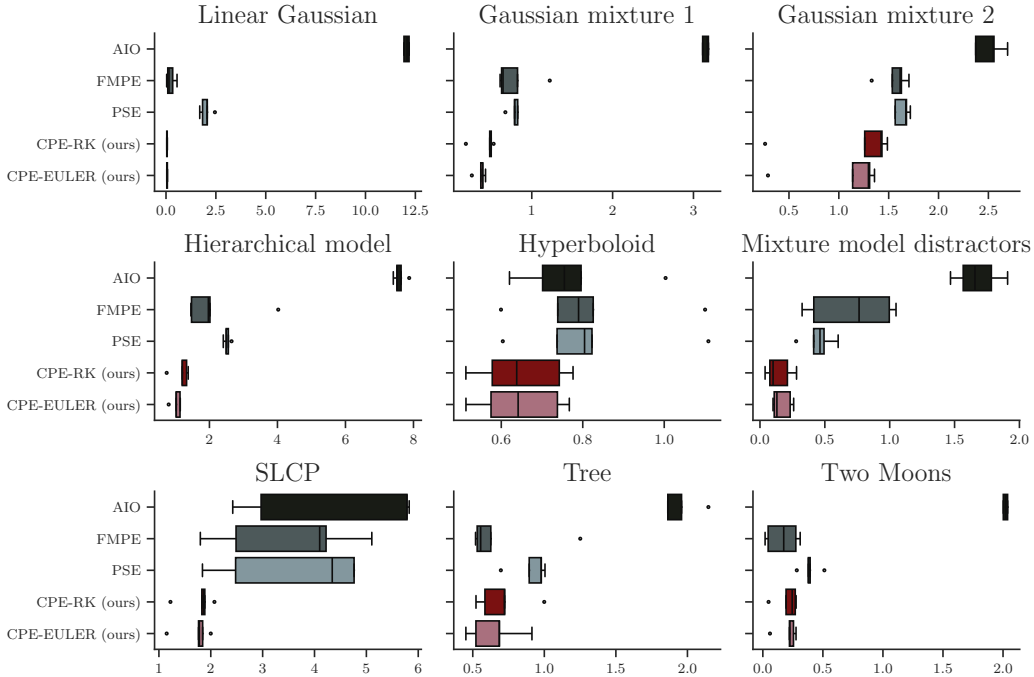


Figure 2: CPE and baseline performance using a H-min metric (smaller values are better). CPE-RK denotes the CPE variant that uses a Runge-Kutta 5(4) solver while CPE-Euler uses a 20-step Euler solver.

performance of the state-of-the-art in all nine experimental models (Figure 2; Appendix D for additional experimental results). Interestingly, the CPE variant that uses an Euler solver using 20 steps (CPE-Euler) is on-par with the variant that does not approximate the ODE trajectory (CPE-RK) and in some cases even outperforms it. This highlights the fact that the rectified training loss (Equation (20)) indeed yields straightened trajectories between

base distribution and posterior, and that the posterior can be sampled efficiently without performance degradation. Moreover, both CPE variants achieve better acceptance rates during posterior sampling than the baselines AIO, FMPE and PSE over all experimental evaluations which can in practice reduce the overall sampling time (Figure 3). We note that CPE achieves this performance while generally having fewer trainable neural network parameters than FMPE and PSE. For instance, compare the 47 000 parameters of CPE in the mixture model with distractors against the 72 000, 191 000 and 191 000 parameters for AIO, FMPE and NPSE, respectively. Similarly, compare the 71 000 parameters of CPE in the hyperboloid, two moons or Gaussian mixture models, against the 71 000, 190 000 and 190 000 for the other baselines.

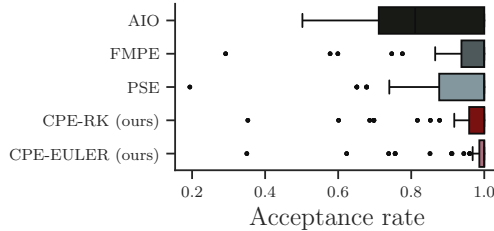


Figure 3: Sampling acceptance rates of all methods. CPE has consistently high acceptance rates when drawing a posterior sample which reduces down the total number of samples required to be drawn. Results from all experimental evaluations (Figure 2) are pooled.

6 Limitations

Our method naturally has several limitations. In particular, the block matrix structure is susceptible to the curse of dimensionality in high-dimensional parameter spaces. While this is negligible when the model involves only a small number of parameters (e.g., on the order of 10), it can become inefficient when hundreds of parameters need to be inferred. Transformer-based methods circumvent this issue by embedding the data and parameters in a fixed-dimensional vector space (Gloeckler et al., 2024; Patacchiola et al., 2024). Future research might elucidate how the expressivity of our approach can be combined with efficient representations. In addition, in this work we are inverting the generative model by naively reversing its edges. This was sufficient for the experimental models in Section 5, but may fail to capture all conditional dependencies correctly (Stuhlmüller et al., 2013; Webb et al., 2018). In future work, we aim to explicitly account for these dependencies to further improve the accuracy of our method. Finally, while efficient algorithms for structured semiseparable matrices exist (Dao & Gu, 2024), in this work we have not enforced a semiseparable structure nor did we make use of these algorithms. Future work could investigate how low-rank structured matrices can be incorporated into SBI methods for increased computational efficiency.

7 Conclusion

We present a simple but powerful approach for SBI called *Causal Posterior Estimation* which effectively incorporates the conditional dependence structure of the prior and posterior programs by that achieving state-of-the-art performance in several benchmark tasks. We

propose both continuous and discrete normalizing flow variants and show that in the continuous case samples can be drawn as quickly as in $\mathcal{O}(1)$ time complexity, thereby matching the sampling efficiency of discrete normalizing flows. Furthermore, we empirically demonstrate that our method achieves near-optimal acceptance rates during posterior sampling, thereby addressing a common limitation of neural SBI methods which often require generating a large number of samples to reach a desired sample size.

Acknowledgements

This research was supported by the Swiss National Science Foundation (Grant No. 200021_208249).

References

- Albergo, M. S., & Vanden-Eijnden, E. (2023). Building normalizing flows with stochastic interpolants. *The Eleventh International Conference on Learning Representations*.
- Albert, C., Künsch, H. R., & Scheidegger, A. (2015). A simulated annealing approach to approximate Bayes computations. *Statistics and Computing*, 25, 1217–1232.
- Albert, C., Ulzega, S., Ozdemir, F., Perez-Cruz, F., & Mira, A. (2022). Learning summary statistics for Bayesian inference with autoencoders. *SciPost Physics Core*, 5(3), 043.
- Ambrogioni, L., Silvestri, G., & van Gerven, M. (2021). Automatic variational inference with cascading flows. *Proceedings of the 38th International Conference on Machine Learning*.
- Babuschkin, I., Baumli et al. (2020). *The DeepMind JAX Ecosystem*.
- Beaumont, M. A., Cornuet, J.-M., Marin, J.-M., & Robert, C. P. (2009). Adaptive approximate Bayesian computation. *Biometrika*, 96(4), 983–990.
- Berner, J., Richter, L., & Ullrich, K. (2024). An optimal control perspective on diffusion-based generative modeling. *Transactions on Machine Learning Research*.
- Blei, D. M., Kucukelbir, A., & McAuliffe, J. D. (2017). Variational inference: A review for statisticians. *Journal of the American statistical Association*, 112(518), 859–877.
- Brooks, S., Gelman, A., Jones, G., & Meng, X.-L. (2011). *Handbook of markov chain monte carlo*. CRC press.
- Chen, R. T., Rubanova, Y., Bettencourt, J., & Duvenaud, D. K. (2018). Neural ordinary differential equations. *Advances in Neural Information Processing Systems*.
- Chen, Y., Gutmann, M. U., & Weller, A. (2023). Is learning summary statistics necessary for likelihood-free inference? *International Conference on Machine Learning*.
- Chen, Y., Zhang, D., Gutmann, M. U., Courville, A., & Zhu, Z. (2021). Neural approximate sufficient statistics for implicit models. *International Conference on Learning Representations*.
- Chung, H., Kim, J., Mccann, M. T., Klasky, M. L., & Ye, J. C. (2023). Diffusion posterior sampling for general noisy inverse problems. *The Eleventh International Conference on Learning Representations*.
- Chung, H., Sim, B., Ryu, D., & Ye, J. C. (2022). Improving diffusion models for inverse problems using manifold constraints. *Advances in Neural Information Processing Systems*.
- Cornish, R., Caterini, A., Deligiannidis, G., & Doucet, A. (2020). Relaxing bijectivity constraints with continuously indexed normalising flows. *Proceedings of the 37th International Conference on Machine Learning*.
- Dao, T., & Gu, A. (2024). Transformers are SSMS: Generalized models and efficient algorithms through structured state space duality. *Forty-first International Conference on Machine Learning*.
- De Bortoli, V., Thornton, J., Heng, J., & Doucet, A. (2021). Diffusion schrödinger bridge with applications to score-based generative modeling. *Advances in Neural Information Processing Systems*, 34.
- De Cao, N., Aziz, W., & Titov, I. (2020). Block neural autoregressive flow. *Proceedings of The 35th Uncertainty in Artificial Intelligence Conference*.
- Deistler, M., Goncalves, P. J., & Macke, J. H. (2022). Truncated proposals for scalable and hassle-free simulation-based inference. In A. H. Oh, A. Agarwal, D. Belgrave, & K. Cho (Eds.), *Advances in neural information processing systems*.
- Del Moral, P., Doucet, A., & Jasra, A. (2012). An adaptive sequential Monte Carlo method for approximate Bayesian computation. *Statistics and Computing*, 22, 1009–1020.

- Delaunoy, A., Hermans, J., Rozet, F., Wehenkel, A., & Louppe, G. (2022). Towards reliable simulation-based inference with balanced neural ratio estimation. *Advances in Neural Information Processing Systems*.
- Dellaporta, C., Knoblauch, J., Damoulas, T., & Briol, F.-X. (2022). Robust bayesian inference for simulator-based models via the mmd posterior bootstrap. *Proceedings of The 25th International Conference on Artificial Intelligence and Statistics*.
- Diaconis, P., & Ylvisaker, D. (1979). Conjugate priors for exponential families. *The Annals of Statistics*, 269–281.
- Dirmeier, S., Albert, C., & Perez-Cruz, F. (2023). Simulation-based inference using surjective sequential neural likelihood estimation. *arXiv preprint arXiv:2308.01054*.
- Dirmeier, S., & Perez-Cruz, F. (2023). Diffusion models for probabilistic programming. *NeurIPS 2023 Workshop on Diffusion Models*.
- Dirmeier, S., Ulzega, S., Mira, A., & Albert, C. (2024). Simulation-based inference with the Python package sbijax. *arXiv preprint arXiv:2409.19435*.
- Dou, Z., & Song, Y. (2024). Diffusion posterior sampling for linear inverse problem solving: A filtering perspective. *The Twelfth International Conference on Learning Representations*.
- Dupont, E., Doucet, A., & Teh, Y. W. (2019). Augmented neural ODEs. *Advances in Neural Information Processing Systems*.
- Durkan, C., Murray, I., & Papamakarios, G. (2020). On contrastive learning for likelihood-free inference. *Proceedings of the 37th International Conference on Machine Learning*.
- Forbes, F., Nguyen, H. D., Nguyen, T., & Arbel, J. (2022). Summary statistics and discrepancy measures for approximate bayesian computation via surrogate posteriors. *Statistics and Computing*, 32(5), 85.
- Frazier, D. T., Robert, C. P., & Rousseau, J. (2020). Model misspecification in approximate Bayesian computation: Consequences and diagnostics. *Journal of the Royal Statistical Society Series B: Statistical Methodology*, 82(2), 421–444.
- Fu, D. Y., Arora, S., Grogan, J., Johnson, I., Eyuboglu, S., Thomas, A. W., Spector, B. F., Poli, M., Rudra, A., & Re, C. (2023). Monarch mixer: A simple sub-quadratic GEMM-based architecture. *Thirty-seventh Conference on Neural Information Processing Systems*.
- Gao, R., Hoogeboom, E., Heek, J., Bortoli, V. D., Murphy, K. P., & Salimans, T. (2025). Diffusion models and gaussian flow matching: Two sides of the same coin. *The Fourth Blogpost Track at ICLR 2025*.
- Geffner, T., & Domke, J. (2023). Langevin diffusion variational inference. *Proceedings of The 26th International Conference on Artificial Intelligence and Statistics*.
- Geffner, T., Papamakarios, G., & Mnih, A. (2023). Compositional score modeling for simulation-based inference. *International Conference on Machine Learning*.
- Germain, M., Gregor, K., Murray, I., & Larochelle, H. (2015). Made: Masked autoencoder for distribution estimation. *Proceedings of the 32nd International Conference on Machine Learning*.
- Glöckler, M., Deistler, M., & Macke, J. H. (2022). Variational methods for simulation-based inference. *International Conference on Learning Representations*.
- Gloekler, M., Deistler, M., & Macke, J. H. (2023). Adversarial robustness of amortized Bayesian inference. *Proceedings of the 40th International Conference on Machine Learning*.
- Gloekler, M., Deistler, M., Weilbach, C. D., Wood, F., & Macke, J. H. (2024). All-in-one simulation-based inference. *Forty-first International Conference on Machine Learning*.

- Greenberg, D., Nonnenmacher, M., & Macke, J. (2019). Automatic posterior transformation for likelihood-free inference. *Proceedings of the 36th International Conference on Machine Learning*.
- Gutmann, M. U., Cor, J., et al. (2016). Bayesian optimization for likelihood-free inference of simulator-based statistical models. *Journal of Machine Learning Research*, 17(125), 1–47.
- Hendrycks, D., & Gimpel, K. (2016). Gaussian error linear units (GELUs). *arXiv preprint arXiv:1606.08415*.
- Hermans, J., Begy, V., & Louppe, G. (2020). Likelihood-free MCMC with amortized approximate ratio estimators. *Proceedings of the 37th International Conference on Machine Learning*.
- Hermans, J., Delaunoy, A., Rozet, F., Wehenkel, A., Begy, V., & Louppe, G. (2022). A crisis in simulation-based inference? beware, your posterior approximations can be unfaithful. *Transactions on Machine Learning Research*.
- Ho, J., Jain, A., & Abbeel, P. (2020). Denoising diffusion probabilistic models. *Advances in Neural Information Processing Systems*.
- Huang, C.-W., Krueger, D., Lacoste, A., & Courville, A. (2018). Neural autoregressive flows. *Proceedings of the 35th International Conference on Machine Learning*.
- Huang, D., Bharti, A., Souza, A., Acerbi, L., & Kaski, S. (2023). Learning robust statistics for simulation-based inference under model misspecification. *Advances in Neural Information Processing Systems*.
- Kadkhodaie, Z., & Simoncelli, E. (2021). Stochastic solutions for linear inverse problems using the prior implicit in a denoiser. *Advances in Neural Information Processing Systems*.
- Karras, T., Aittala, M., Aila, T., & Laine, S. (2022). Elucidating the design space of diffusion-based generative models. *Advances in Neural Information Processing Systems*.
- Katharopoulos, A., Vyas, A., Pappas, N., & Fleuret, F. (2020). Transformers are RNNs: Fast autoregressive transformers with linear attention. *Proceedings of the 37th International Conference on Machine Learning*.
- Kawar, B., Elad, M., Ermon, S., & Song, J. (2022). Denoising diffusion restoration models. *Advances in Neural Information Processing Systems*.
- Kawar, B., Vaksman, G., & Elad, M. (2021). SNIPS: Solving noisy inverse problems stochastically. *Advances in Neural Information Processing Systems*.
- Kelly, R. P., Nott, D. J., Frazier, D. T., Warne, D. J., & Drovandi, C. (2024). Misspecification-robust sequential neural likelihood for simulation-based inference. *Transactions on Machine Learning Research*.
- Kingma, D. P., & Ba, J. (2015). Adam: A method for stochastic optimization. *International Conference on Learning Representations*.
- Kingma, D. P., Salimans, T., Jozefowicz, R., Chen, X., Sutskever, I., & Welling, M. (2016). Improved variational inference with inverse autoregressive flow. *Advances in Neural Information Processing Systems*.
- Köster, J., & Rahmann, S. (2012). Snakemake—a scalable bioinformatics workflow engine. *Bioinformatics*, 28(19), 2520–2522.
- Kumar, R., Carroll, C., Hartikainen, A., & Martin, O. (2019). Arviz a unified library for exploratory analysis of Bayesian models in Python. *Journal of Open Source Software*, 4(33), 1143.
- Lipman, Y., Chen, R. T. Q., Ben-Hamu, H., Nickel, M., & Le, M. (2023). Flow matching for generative modeling. *The Eleventh International Conference on Learning Representations*.

- Liu, X., Gong, C., & qiang liu. (2023). Flow straight and fast: Learning to generate and transfer data with rectified flow. *The Eleventh International Conference on Learning Representations*.
- Lopez-Paz, D., & Oquab, M. (2017). Revisiting classifier two-sample tests. *International Conference on Learning Representations*.
- Lueckmann, J.-M., Boelts, J., Greenberg, D., Goncalves, P., & Macke, J. (2021). Benchmarking simulation-based inference. *Proceedings of the 24th International Conference on Artificial Intelligence and Statistics*.
- Lueckmann, J.-M., Goncalves, P. J., Bassetto, G., Öcal, K., Nonnenmacher, M., & Macke, J. H. (2017). Flexible statistical inference for mechanistic models of neural dynamics. *Advances in Neural Information Processing Systems*.
- Miller, B. K., Weniger, C., & Forré, P. (2022). Contrastive neural ratio estimation. *Advances in Neural Information Processing Systems*.
- Pacchiardi, L., & Dutta, R. (2022). Score matched neural exponential families for likelihood-free inference. *The Journal of Machine Learning Research*, 23(1), 1745–1815.
- Papamakarios, G., & Murray, I. (2016). Fast ε -free inference of simulation models with Bayesian conditional density estimation. *Advances in Neural Information Processing Systems*, 29.
- Papamakarios, G., Pavlakou, T., & Murray, I. (2017). Masked autoregressive flow for density estimation. *Advances in Neural Information Processing Systems*.
- Papamakarios, G., Sterratt, D., & Murray, I. (2019). Sequential neural likelihood: Fast likelihood-free inference with autoregressive flows. *Proceedings of the 22nd International Conference on Artificial Intelligence and Statistics*.
- Patacchiola, M., Shysheya, A., Hofmann, K., & Turner, R. E. (2024). Transformer neural autoregressive flows. *ICML 2024 Workshop on Structured Probabilistic Inference & Generative Modeling*.
- Radev, S. T., Schmitt, M., Pratz, V., Picchini, U., Köthe, U., & Bürkner, P.-C. (2023). Jana: Jointly amortized neural approximation of complex Bayesian models. *Proceedings of the Thirty-Ninth Conference on Uncertainty in Artificial Intelligence*.
- Rout, L., Raoof, N., Daras, G., Caramanis, C., Dimakis, A., & Shakkottai, S. (2023). Solving linear inverse problems provably via posterior sampling with latent diffusion models. *Thirty-seventh Conference on Neural Information Processing Systems*.
- Schmitt, M., Pratz, V., Köthe, U., Bürkner, P.-C., & Radev, S. T. (2024). Consistency models for scalable and fast simulation-based inference. *Advances in Neural Information Processing Systems*.
- Sharrock, L., Simons, J., Liu, S., & Beaumont, M. (2024). Sequential neural score estimation: Likelihood-free inference with conditional score based diffusion models. *Forty-first International Conference on Machine Learning*.
- Sisson, S. A., Fan, Y., & Beaumont, M. (2018). *Handbook of approximate bayesian computation*. CRC Press.
- Song, Y., Dhariwal, P., Chen, M., & Sutskever, I. (2023). Consistency models. *Proceedings of the 40th International Conference on Machine Learning*.
- Song, Y., & Ermon, S. (2019). Generative modeling by estimating gradients of the data distribution. *Advances in Neural Information Processing Systems*.
- Song, Y., Sohl-Dickstein, J., Kingma, D. P., Kumar, A., Ermon, S., & Poole, B. (2021). Score-based generative modeling through stochastic differential equations. *International Conference on Learning Representations*.
- Stuhlmüller, A., Taylor, J., & Goodman, N. (2013). Learning stochastic inverses. *Advances in Neural Information Processing Systems*.

- Tancik, M., Srinivasan, P., Mildenhall, B., Fridovich-Keil, S., Raghavan, N., Singhal, U., Ramamoorthi, R., Barron, J., & Ng, R. (2020). Fourier features let networks learn high frequency functions in low dimensional domains. *Advances in Neural Information Processing Systems*.
- Tong, A., Fatras, K., Malkin, N., Huguët, G., Zhang, Y., Rector-Brooks, J., Wolf, G., & Bengio, Y. (2024). Improving and generalizing flow-based generative models with minibatch optimal transport. *Transactions on Machine Learning Research*.
- Tong, A. Y., Malkin, N., Fatras, K., Atanackovic, L., Zhang, Y., Huguët, G., Wolf, G., & Bengio, Y. (2024). Simulation-free Schrödinger bridges via score and flow matching. *Proceedings of The 27th International Conference on Artificial Intelligence and Statistics*.
- van de Meent, J.-W., Paige, B., Yang, H., & Wood, F. (2018). An introduction to probabilistic programming. *arXiv preprint arXiv:1809.10756*.
- Vargas, F., Grathwohl, W. S., & Doucet, A. (2023). Denoising diffusion samplers. *The Eleventh International Conference on Learning Representations*.
- Vargas, F., Ovsianas, A., Fernandes, D. L., Girolami, M., Lawrence, N. D., & Nüsken, N. (2022). Bayesian learning via neural Schrödinger-Föllmer flows. *Fourth Symposium on Advances in Approximate Bayesian Inference*.
- Vargas, F., Padhy, S., Blessing, D., & Nüsken, N. (2024). Transport meets variational inference: Controlled Monte Carlo diffusions. *The Twelfth International Conference on Learning Representations*.
- Vaswani, A., Shazeer, N., Parmar, N., Uszkoreit, J., Jones, L., Gomez, A. N., Kaiser, Ł., & Polosukhin, I. (2017). Attention is all you need. *Advances in Neural Information Processing Systems*, 30.
- Vehtari, A., Gelman, A., Simpson, D., Carpenter, B., & Bürkner, P.-C. (2021). Rank-normalization, folding, and localization: An improved \hat{R} for assessing convergence of MCMC. *Bayesian analysis*, 16(2), 667–718.
- Verma, Y., Bharti, A., & Garg, V. (2025). Robust simulation-based inference under missing data via neural processes. *The Thirteenth International Conference on Learning Representations*.
- Virtanen, P., Gommers, R., Oliphant, T. E., Haberland, M., Reddy, T., Cournapeau, D., Burovski, E., Peterson, P., Weckesser, W., Bright, J., van der Walt, S. J., Brett, M., Wilson, J., Millman, K. J., Mayorov, N., Nelson, A. R. J., Jones, E., Kern, R., Larson, E., ... SciPy 1.0 Contributors. (2020). SciPy 1.0: Fundamental Algorithms for Scientific Computing in Python. *Nature Methods*, 17, 261–272.
- Ward, D., Cannon, P., Beaumont, M., Fasiolo, M., & Schmon, S. (2022). Robust neural posterior estimation and statistical model criticism. *Advances in Neural Information Processing Systems*.
- Webb, S., Golinski, A., Zinkov, R., Rainforth, T., Teh, Y. W., Wood, F., et al. (2018). Faithful inversion of generative models for effective amortized inference. *Advances in Neural Information Processing Systems*.
- Wildberger, J. B., Dax, M., Buchholz, S., Green, S. R., Macke, J. H., & Schölkopf, B. (2023). Flow matching for scalable simulation-based inference. *Thirty-seventh Conference on Neural Information Processing Systems*.
- Yuyan, W., Evans, M., & Nott, D. J. (2025). Robust bayesian methods using amortized simulation-based inference. *arXiv preprint arXiv:2504.09475*.
- Zhang, Q., & Chen, Y. (2022). Path integral sampler: A stochastic control approach for sampling. *International Conference on Learning Representations*.

Zhao, S., Sinha, A., He, Y., Perreault, A., Song, J., & Ermon, S. (2022). Comparing distributions by measuring differences that affect decision making. *International Conference on Learning Representations*.

A Model details

CPE is a normalizing-flow based neural posterior method. Below, we describe both CPE variants and required background.

A.1 CPE with continuous normalizing flows

A.1.1 Continuous normalizing flows

In the following, we give background on continuous normalizing flows and flow matching. Similar expositions can be found in R. T. Chen et al. (2018), Lipman et al. (2023), and Liu et al. (2023).

In *Flow Matching*, we aim to find a probability density path ϱ_t that starts at an arbitrary base distribution $\varrho_0 = \pi_{\text{base}}(\theta)$, i.e., a standard Gaussian, and ends in a distribution ϱ_1 that closely approximates the distribution that we are interested in sampling from $\pi(\theta)$, i.e., $\varrho_1(\theta) \approx \pi(\theta)$. The density path ϱ_t is constructed via a vector field u_t that defines the ODE

$$\frac{\partial \Lambda_t}{\partial t} = u_t(\Lambda_t) \quad (21)$$

$$\Lambda_0 = \theta^{(0)} \quad (22)$$

where we sample $\theta^{(0)} \sim \pi_{\text{base}}(\theta)$. Assuming the probability density path ϱ_t and the corresponding vector field u_t that induces it are given, the vector field can be approximated numerically with a neural network $v_{t,\phi}(\theta)$ using a simple least-squared error loss

$$\hat{\phi} = \arg \min_{\phi} \mathbb{E}_{t \sim \mathcal{U}(0,1), \theta^{(t)} \sim \varrho_t(\theta)} \left[\|v_{t,\phi}(\theta^{(t)}) - u_t(\theta^{(t)})\|^2 \right] \quad (23)$$

In practice, both the vector field u_t and density paths ϱ_t are, however, not given and solutions for u_t that generate ϱ_t might be intractable. One convenient way is to define the density path on a *per-sample* basis as a continuous mixture

$$\varrho_t(\theta) = \int \varrho_t(\theta|\theta^{(1)})\pi(\theta^{(1)})d\theta^{(1)} \quad (24)$$

using conditional distributions $\varrho_t(\theta|\theta^{(1)})$ and a data sample $\theta^{(1)} \sim \pi(\theta)$. We construct the conditional distributions such that they satisfy $\varrho_0(\theta|\theta^{(1)}) = \pi_{\text{base}}$ and $\mathbb{E}_{\varrho_1(\theta|\theta^{(1)})} = \theta^{(1)}$. If $\varrho_1(\theta|\theta^{(1)})$ has also sufficiently small variance, the marginal $\varrho_1(\theta)$ closely approximates the data distribution

$$\pi(\theta) \approx \varrho_1(\theta) = \int \varrho_1(\theta|\theta^{(1)})\pi(\theta^{(1)})d\theta^{(1)}$$

This construction is not yet particularly useful. However, as Lipman et al. (2023) show one can similarly define a conditional vector field $u_t(\cdot|\theta^{(1)})$ that generates ϱ_t and which is related to the *marginal* vector field u_t via

$$u_t(\theta) = \int u_t(\theta|\theta^{(1)}) \frac{\varrho(\theta|\theta^{(1)})\pi(\theta^{(1)})}{\varrho_t(\theta)} d\theta^{(1)} \quad (25)$$

This construction allows us to construct u_t (and ϱ_t) via $u_t(\cdot|\theta^{(1)})$ (and $\varrho_t(\cdot|\theta^{(1)})$, respectively) which Lipman et al. (2023) formalize as below:

Theorem 1. *Given vector fields $u_t(\theta|\theta^{(1)})$ that generate conditional probability paths $\varrho_t(\theta|\theta^{(1)})$, for any distribution $\pi(\theta^{(1)})$, the marginal vector field u_t in Equation (25) generates the marginal probability path ϱ_t in Equation (24).*

Proof. It suffices to check that ϱ_t and u_t satisfy the continuity equation:

$$\begin{aligned} \frac{d}{dt}\varrho_t(\theta) &= \int \left(\frac{d}{dt}\varrho_t(\theta|\theta^{(1)}) \right) \pi(\theta^{(1)})d\theta^{(1)} \\ &= - \int \operatorname{div} \left(u_t(\theta|\theta^{(1)})\varrho_t(\theta|\theta^{(1)}) \right) \pi(\theta^{(1)})d\theta^{(1)} \\ &= -\operatorname{div} \left(\int u_t(\theta|\theta^{(1)})\varrho_t(\theta|\theta^{(1)})\pi(\theta^{(1)})d\theta^{(1)} \right) \\ &= -\operatorname{div} (u_t(\theta)\varrho_t(\theta)) \end{aligned}$$

□

and where the continuity equation is defined as

$$\frac{d}{dt}\varrho_t(\theta) = -\operatorname{div} (\varrho_t(\theta)v_t(\theta))$$

We can now define a novel tractable flow matching objective that is defined on a per-sample basis and consequently easy to compute

$$\hat{\phi} = \arg \min_{\phi} \mathbb{E}_{t \sim \mathcal{U}(0,1), \theta^{(1)} \sim \pi(\theta), \theta^{(t)} \sim \varrho_t(\theta|\theta^{(1)})} \left[\|v_{t,\phi}(\theta^{(t)}) - u_t(\theta^{(t)}|\theta^{(1)})\|^2 \right]$$

Surprisingly, this objective has the same optima and the same gradients as the initial objective (similarly to denoising score matching (Song & Ermon, 2019)) and can be used in lieu of original objective in Equation 23.

Lipman et al. (2023) define a particularly useful parameterization for the conditional density path based on Gaussian transition kernels and the respective conditional vector field:

$$\begin{aligned} \varrho_t(\theta|\theta^{(1)}) &= \mathcal{N}(t\theta^{(1)}, (1 - (1 - \sigma_{\min})t)^2 I) \\ u_t(\theta|\theta^{(1)}) &= \frac{\theta_1 - (1 - \sigma_{\min})\theta}{1 - (1 - \sigma_{\min})\theta} \end{aligned} \tag{26}$$

where σ_{\min} is a hyperparameter (see the original publication for details) and which is the optimal displacement map between $\varrho_0(\theta|\theta^{(1)})$ and $\varrho_1(\theta|\theta^{(1)})$ which has the practical properties that sampled particles always move in a straight line.

In our case, we instead choose the (also straight) transport map defined via

$$\begin{aligned} \varrho_t(\theta|\theta^{(1)}, \theta^{(0)}) &= t\theta^{(1)} - (1 - t)\theta^{(0)} \\ u_t(\theta|\theta^{(1)}, \theta^{(0)}) &= \theta^{(1)} - \theta^{(0)} \end{aligned} \tag{27}$$

Since $\theta^{(t)}$ is in this case not (necessarily) Gaussian as in Equation 26, we can choose arbitrary base distributions π_{base} which will become useful in the Section A.1.2.

A.1.2 Neural posterior estimation

To make flow matching useful for neural posterior estimation, we aim to find an approximation to the posterior $\pi(\theta|x)$. For that purpose, we first need to define the vector

field v_t on a conditional basis, i.e., we define the network to take an additional input x : $v : [0, 1] \times \mathbb{R}^{d_\theta} \times \mathbb{R}^{d_x}$.

Adopting the objective from Wildberger et al. (2023), to approximate the posterior distribution we then train the vector field by minimizing the least-squares loss

$$\hat{\phi} = \arg \min_{\phi} \mathbb{E} \left[\|v_t(\theta^{(t)}, x) - u_t(\theta^{(t)} | \theta^{(1)}, \theta^{(0)})\|^2 \right]$$

where the expectation is taken w.r.t. $t \sim \mathcal{U}(0, 1)$, $\theta^{(1)} \sim \pi(\theta)$, $\theta^{(0)} \sim \pi_{\text{base}}(\theta)$, $x \sim \pi(x | \theta^{(1)})$, $\theta^{(t)} \sim \varrho_t(\theta | \theta^{(1)})$ and where we replace the expectation w.r.t. $\pi(x)\pi(\theta|x)$ with the equivalent $\pi(\theta)\pi(x|\theta)$.

Utilizing the linear transport map in Equation 27, the objective becomes

$$\hat{\phi} = \arg \min_{\phi} \mathbb{E} \left[\|v_t(\theta^{(t)}, x) - (\theta^{(1)} - \theta^{(0)})\|^2 \right]$$

A.1.3 Architecture

In the continuous case, the vector field is a function of time, parameters and data $v : [0, 1] \times \mathbb{R}^{d_\theta} \times \mathbb{R}^{d_x}$. The activation functions act and g can be arbitrary in this case, since we do not require the network to be invertible. See Figure 4 for an overview.

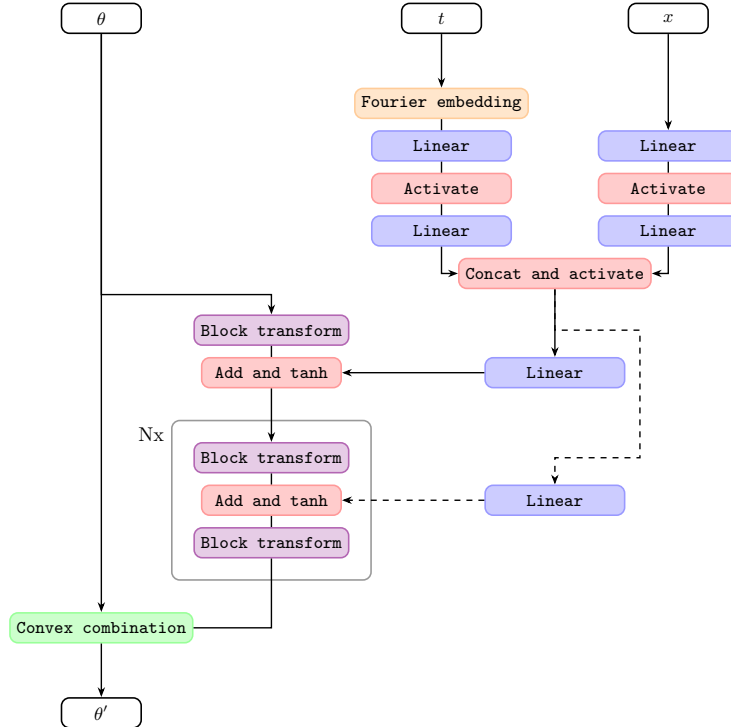


Figure 4: Continuous-time CPE architecture. Data x and time t are preprocessed using an MLP and a Fourier embedding + MLP, respectively, concatenated and used as conditioning variables. We condition after a block transform before applying an activation function (Equation (18)). While it is possible to do the conditioning after each block transform (dashed lines), here, we only do it after the first projection. In the end, to account for the prior program, we apply a convex combination (Equation (13)).

A.2 CPE with discrete normalizing flows

A.2.1 Discrete normalizing flows

As CNFs, "discrete" NFs define probability distributions in terms of a diffeomorphism Λ and an arbitrary base distribution $\pi_{\text{base}}(\theta)$:

$$\begin{aligned} q(\theta) &= T_{\Lambda}[\pi_{\text{base}}](\theta) \\ &= \pi_{\text{base}}\left(\Lambda^{-1}(\theta)\right) \left| \det \frac{\partial \Lambda^{-1}(\theta)}{\partial \theta} \right| \end{aligned} \quad (28)$$

where T_{Λ} is a pushforward measure, T is the pushforward operator associated with the mapping $\Lambda : \mathbb{R}^{d_{\theta}} \rightarrow \mathbb{R}^{d_{\theta}}$, and the second term on the right-hand side is the absolute value of the Jacobian determinant.

To be able to compute the determinant effectively, we require the Jacobian to have a lower-triangular shape. In that case, such the determinant can be computed by simply multiplying the trace elements of the Jacobian. The family of autoregressive flows (which our block transform is part of due to its autoregressive factorization) fulfills this requirement naturally. For the transformation $f^{(k)}$, we set all weights on the block-diagonal to strictly positive values by transforming all values through a strictly-positive transformation $g := \exp$. This ensures monotonicity and hence invertibility. On the lower-triangular off-block diagonal this requirement is not necessary. As mentioned before, it is also required that all activations act are invertible which is the case for, e.g., tanh, LeakyReLUs, LeakyTanh, etc. activations. Here we employ tanh activations.

The Jacobian determinant of a sequence of block transformations $f = f^{(K)} \circ \dots \circ f^{(1)}$ (Equation 18) can be computed via the chain rule:

$$\begin{aligned} \log \left| \det \frac{\partial f}{\partial \theta} \right| &= \sum_{i=1}^{d_{\theta}} \log \left(\frac{\partial f}{\partial \theta} \right)_{ii} \\ &= \sum_{i=1}^{d_{\theta}} \log \left(\frac{\partial f^{(K)}}{\partial f^{(K-1)}} \frac{\partial f^{(K-1)}}{\partial f^{(K-2)}} \dots \frac{\partial f^{(1)}}{\partial \theta} \right)_{ii} \\ &= \sum_{i=1}^{d_{\theta}} \log g(B_{ii}^{(K)}) \star \log \frac{\partial \text{act}}{h_i^{(K-2)}} \star \dots \star \log g(B_{ii}^{(1)}) \end{aligned}$$

where B_{ii} are matrices (see Section 3.2) and $h_i^{(K-2)}$ the diagonal elements of the output of function $f^{(K-2)}$ which depend on θ_i , and where we denote with \star the log-matrix multiplication which we can be implemented as

$$\log A \star \log B = \log \sum_{k=1}^n \exp(A_{ik} + B_{kj})$$

A.2.2 Neural posterior estimation

In comparison to the discrete case, the discrete NF training objective does not solving an ODE and hence can be done using maximum likelihood (ML). We first construct the pushforward on a conditional basis, i.e.,

$$q(\theta, x) = \pi_{\text{base}}\left(\Lambda^{-1}(\theta, x)\right) \left| \det \frac{\partial \Lambda^{-1}(\theta, x)}{\partial \theta} \right| \quad (29)$$

where Λ is an invertible transformation given data x . Then, following the discrete NPE literature (e.g., (Greenberg et al., 2019)) we use the ML objective

$$\hat{\phi} = \arg \max_{\phi} \mathbb{E}_{\theta \sim \pi(\theta), x \sim \pi(x|\theta)} [q(\theta, x)] \quad (30)$$

With a trained normalizing flow, sampling from the posterior is as simple as drawing $\theta \sim \pi_{\text{base}}(\theta)$ and then pushing the sample through the transform Λ . However, since the flow does not have an analytical inverse, we first need to find it by, e.g., bifurcation.

A.2.3 Architecture

In the discrete case, we drop the time argument from the vector field and define it as $v : \mathbb{R}^{d_\theta} \times \mathbb{R}^{d_x}$. In Figure 4, this would correspond to the t -block being deleted. The resulting architecture is invertible given x .

B Experimental models

We evaluate CPE on benchmark models from the recent literature (Forbes et al., 2022; Gloeckler et al., 2024; Greenberg et al., 2019; Lueckmann et al., 2021; Papamakarios et al., 2019; Vargas et al., 2024) and develop new benchmark tasks. We describe the different models below.

B.1 Linear Gaussian

The linear Gaussian benchmark task is defined by the following generative process:

$$\theta \sim \mathcal{N}_{10}(0, \sigma^2 I) \quad (31)$$

$$x | \theta \sim \mathcal{N}_{10}(\theta, \sigma^2 I) \quad (32)$$

where $\sigma^2 = 0.1$, I is a unit matrix of appropriate dimensionality, and both $\theta \in \mathbb{R}^{10}$ and $x \in \mathbb{R}^{10}$ are ten-dimensional random variables. The linear Gaussian follows the representation in Lueckmann et al. (2021).

B.2 Gaussian mixture 1

The Gaussian mixture 1 has the following generative process:

$$\theta \sim \mathcal{U}_2(-10, 10)$$

$$x | \theta \sim \frac{1}{2} \mathcal{N}_2(\theta, I) + \frac{1}{2} \mathcal{N}_2(\theta, \sigma^2 I)$$

where $\sigma^2 = 0.01$, I is a unit matrix, and both $\theta \in \mathbb{R}^2$ and $x \in \mathbb{R}^2$ are two-dimensional random variables. The GMM follows the representation in Lueckmann et al. (2021).

B.3 Gaussian mixture 2

The Gaussian mixture 2 has been proposed in Vargas et al. (2024). It is a 3-component mixture that we adapted for SBI. It has the following generative process:

$$\theta \sim \mathcal{N}_6 \left([-1, -1, 0, 0, 1, 1]^T, I \right)$$

$$x | \theta \sim \frac{1}{3} \mathcal{N}_2 \left(\theta_{1,2}, \begin{bmatrix} 0.7 & 0 \\ 0 & 0.05 \end{bmatrix} \right) + \frac{1}{3} \mathcal{N}_2 \left(\theta_{3,4}, \begin{bmatrix} 0.7 & 0 \\ 0 & 0.05 \end{bmatrix} \right) + \frac{1}{3} \mathcal{N}_2 \left(\theta_{5,6}, \begin{bmatrix} 0.1 & 0.95 \\ 0.95 & 1 \end{bmatrix} \right)$$

where I is a unit matrix, and $\theta \in \mathbb{R}^6$ and $x \in \mathbb{R}^2$ are six- and two-dimensional random variables, respectively.

B.4 Hierarchical model

We propose a novel hierarchical model for benchmarks in SBI. The model has the following generative process:

$$\gamma \sim \mathcal{N}_2(0, I)$$

$$\beta_1, \beta_2, \beta_3 \sim \mathcal{N}_2(\gamma, I)$$

$$\sigma \sim \mathcal{N}^+(1)$$

$$x | \beta \sim \mathcal{N} \left([\beta_1, \beta_2, \beta_3]^T, \sigma^2 I \right)$$

where $\theta = (\gamma, \beta_1, \beta_2, \beta_3, \sigma)$ is a seven-dimensional random variable for which the posterior should be inferred, I is a unit matrix, and $x \in \mathbb{R}^6$.

B.5 Hyperboloid

The hyperboloid model (Forbes et al., 2022) is a 2-component mixture of Student's t -distributions of the form

$$\theta \sim \mathcal{U}_2(-2, 2) \quad (33)$$

$$x \mid \theta \sim \frac{1}{2}t_{10}(\nu, F(\theta; a_1, a_2)\mathbb{I}, \sigma^2 I) + \frac{1}{2}t_{10}(\nu, F(\theta; b_1, b_2)\mathbb{I}, \sigma^2 I) \quad (34)$$

which are parameterized by degrees of freedom ν , mean

$$F(\theta; x_1, x_2) = \text{abs}(\|\theta - x_1\|_2 - \|\theta - x_2\|_2),$$

and scale matrix $\sigma^2 I$. \mathbb{I} is a ten-dimensional vector of ones. We follow Forbes et al. (2022) and set $a_1 = [-0.5, 0.0]^T$, $a_2 = [0.5, 0.0]^T$, $b_1 = [0.0, -0.5]^T$, $b_2 = [0.0, 0.5]^T$, $\nu = 3$ and $\sigma^2 = 0.01$ for our experiments.

B.6 Mixture model with distractors

Similarly to the SLCP task (Lueckmann et al., 2021), we evaluate a benchmark task that uses distractor dimensions appending the data with dimensions that are not informative of the parameters. The generative process of the model is as follows:

$$\begin{aligned} \theta &\sim \mathcal{U}(-10, 10) \\ x_1, x_2 &\sim \alpha \mathcal{N}(\theta, 1) + (1 - \alpha) \mathcal{N}(-\theta, \sigma^2) \\ x_3, \dots, x_{10} &\sim \mathcal{N}(0, 1) \end{aligned}$$

where we set $\alpha = \sigma = 0.3$. In addition to the two informative data dimensions x_1, x_2 , the model adds 8 samples from a standard Gaussian that do not carry information of the parameters. If both $x_{1,obs}$ and $x_{2,obs}$ are from the same mode (in our experiments we set $x_{1,obs} = x_{2,obs} = 5$), then the posterior for θ is bimodal with very uneven mass distribution.

B.7 SLCP

The "simple likelihood complex posterior" model is a frequent benchmark model in the SBI literature (Papamakarios et al., 2019). Its generative process is as follows:

$$\begin{aligned} \theta_i &\sim \text{Uniform}(-3, 3) \text{ for } i = 1, \dots, 5 \\ \mu(\theta) &= (\theta_1, \theta_2), \phi_1 = \theta_3^2, \phi_2 = \theta_4^2 \\ \Sigma(\theta) &= \begin{pmatrix} \phi_1^2 & \tanh(\theta_5)\phi_1\phi_2 \\ \tanh(\theta_5)\phi_1\phi_2 & \phi_2^2 \end{pmatrix} \\ x_j \mid \theta &\sim \mathcal{N}(x_j; \mu(\theta), \Sigma(\theta)) \text{ for } j = 1, \dots, 4 \\ x &= [x_1, \dots, x_4]^T \end{aligned}$$

Hence $\theta \in \mathbb{R}^5$ is a five-dimensional random variable, while the data x has eight dimensions.

B.8 Tree

The tree model is a recently introduced SBI benchmark model (Gloeckler et al., 2024). It has the following generative process:

$$\begin{aligned}\theta_1 &\sim \mathcal{N}(0, 1) \\ \theta_2 &\sim \mathcal{N}(\theta_1, 1) \\ \theta_3 &\sim \mathcal{N}(\theta_1, 1) \\ x_1 &\sim \mathcal{N}\left(\sin(\theta_2)^2, 0.2^2\right) \\ x_2 &\sim \mathcal{N}\left(\theta_2^2, 0.2^2\right) \\ x_2 &\sim \mathcal{N}\left(0.1\theta_3^2, 0.6^2\right) \\ x_3 &\sim \mathcal{N}\left(\cos(\theta_3)^2, 0.1^2\right)\end{aligned}$$

B.9 Two moons

Two moons is a common benchmark task in the SBI literature (Greenberg et al., 2019). Its generative process is defined as:

$$\begin{aligned}\theta &\sim \mathcal{U}_2(-10, 10) \\ \alpha &\sim \mathcal{U}(-\pi/2, \pi/2) \\ r &\sim \mathcal{N}(0.1, 0.1^2) \\ x \mid \theta &= \begin{pmatrix} r \cos \alpha + 0.25 \\ r \sin \alpha \end{pmatrix} + \begin{pmatrix} -|\theta_1 + \theta_2|/\sqrt{2} \\ -(\theta_1 + \theta_2)/\sqrt{2} \end{pmatrix},\end{aligned}$$

where we treat α and r as nuisance parameters.

C Experimental details

In the following, we describe the experimental details for each benchmark task and inferential algorithm. All source code to reproduce our results can be found in the supplemental material and on GitHub (link published after review period).

C.1 Reference posterior distributions

We use the Python package `sbijax` (Dirmeier et al., 2024) to draw reference, i.e., "ground-truth" posterior samples using different Markov Chain Monte Carlo samplers. For all experimental models, we sample on 10 independent MCMC chains 10 000 samples of which we discard the first 5 000 as warmup. In addition, we used a thinned the MCMC chain such that only every second sample is accepted to reduce autocorrelation. Hence, the reference posterior sample consists of 50 00 particles. We used a hit-and-run Slice Sampler (SS) for the models "Gaussian linear", "Gaussian Mixture 1", "Gaussian Mixture 2", "Hierarchical Model", "Hyperboloid", "Mixture Model with Distractors", "SLCP", "Tree" and "Two Moons". We monitored convergence using the typical MCMC diagnostic tools, i.e., the rank normalized split \hat{R} (Vehtari et al., 2021) and effective sample size as implemented in the Python package Kumar et al. (2019).

C.2 Comparing reference posteriors to inferred posteriors

We compare the inferred posterior distributions to the reference posterior distributions using the classifier-two-sample-test statistic (C2ST, Lopez-Paz and Oquab (2017)) and the recently introduced H-Min divergence (Zhao et al., 2022) which we, like Dirmeier, Albert, and Perez-Cruz (2023), found to be easier to tune than C2ST and other divergences. To compute the metrics, we first subsample both reference and inferred posteriors to 10 000 samples, and then compute both metrics.

C.3 Neural network architectures

For AIO, FMPE and PSE we use implementations from the Python package `sbi_jax` (Dirmeier et al., 2024). The neural network architectures of CPE and all baselines are detailed below.

CPE CPE is structured as a block neural autoregressive flow. We first embed time variables t using a Fourier projection using 64 Fourier features and then embed the features using a two-layer MLP with 64 nodes each. We then project the data variables x through a two-layer MLP with 128 nodes each. We then concatenate the embeddings of time t and data x before projecting the resulting vector and the parameter values θ through the transformations $f = (f^{(1)}, \dots, f^{(K)})$. In our experiments, we set $K = 3$ and use a block size of 64 meaning we set

$$\begin{aligned}d_{\text{in}}^{(1)} &= 1, d_{\text{out}}^{(1)} = 64 \\d_{\text{in}}^{(2)} &= 64, d_{\text{out}}^{(2)} = 64 \\d_{\text{in}}^{(3)} &= 64, d_{\text{out}}^{(3)} = 64 \\d_{\text{in}}^{(4)} &= 64, d_{\text{out}}^{(4)} = 1\end{aligned}$$

Each $f^{(k)}$ is then designed as described in Equation (18), where we use \tanh activation functions $\text{act} := \tanh$ and the identity function for g . We condition on data and time, by adding concatenation of the data and time embeddings after the first projection $f^{(1)}$, i.e.,

$$\begin{aligned}\theta' &= f^{(1)}(\theta) \\ \theta'' &= \theta' + \text{Linear}(c)\end{aligned}$$

where we denote with `Linear` a linear neural network layer (with bias) and with c the concatenation of time and data embeddings. We denote with λ_t the initial embedding and consecutive the projection through the blocks f . The result of these operations are projected through a convex combination as described in Equation (13). The

AIO As in the original publication (Gloeckler et al., 2024), AIO uses a transformer backbone as a score model. In order to use roughly the same number of parameters as CPE, we only use one layer and one attention head for all experiments. We used embedding dimensions of 32, 32 and 8 for values, ids and conditioning variables, respectively. We used an MLP with two layers of 64 nodes each as time embedding. We used a dropout rate of 0.0. All activation functions are SiLUs (Hendrycks & Gimpel, 2016). AIO uses the variance preserving-SDE of Song et al. (2021) using a minimum scale of $\sigma_{\text{min}} = 0.1$ and maximum scale of $\sigma_{\text{max}} = 10$. To faithfully compare AIO against CPE, we use directed graphs as masks for AIO.

FMPE FMPE uses a two-layer MLP with 128 nodes each to embed parameter values θ and a two-layer MLP with 128 nodes each to embed data values x . We first project time values t through random Fourier features of dimensionality 64, before embedding the result using a two-layer MLP with 64 nodes each. We then concatenate embedded parameter, data and time values θ , x and t , respectively, and projecting them through an MLP with two hidden layers and 256 nodes per layers. FMPE uses the forward process and vector field as described in Lipman et al. (2023) and we set $\sigma_{\min} = 0.001$. All activation functions are SiLUs (Hendrycks & Gimpel, 2016).

PSE We use the same neural network architecture as for FMPE (since the mathematical frameworks are the same). PSE uses the variance-preserving SDE of Song et al. (2021) using a minimum scaled of $\sigma_{\min} = 0.1$ and maximum scale of $\sigma_{\max} = 10$. All activation functions are SiLUs (Hendrycks & Gimpel, 2016).

C.4 Training

Each neural SBI method (i.e., CPE and all baselines) are trained using an Adam optimizer (Kingma & Ba, 2015) with learning rate $lr = 0.0001$ and $\beta_1 = 0.9$ and $\beta_2 = 0.999$. We trained each method to convergence with a maximum of 2 000 training epochs (whichever is fulfilled first). We used 10% of the simulated data as a validation set. We use `Optax` for gradient-based optimization (Babuschkin, Baumli, et al., 2020).

C.5 Sampling

We sample from the posterior distribution of each method using a Runge-Kutta 5(4) solver. For the benchmark models, we use the implementations of `sbijax` (Dirmeier et al., 2024).

For the CPE variant CPE-RK, we use the Runge-Kutta 5(4) implementation of `SciPy` (Virtanen et al., 2020) with default parameters. For the CPE variant CPE-Euler, we use a custom Euler solver with $T = 20$ steps and discretization $dt = \frac{1}{20}$.

C.6 Computational resources

All MCMC sampling, model training and model evaluations were run on an AMD EPYC7M 7742 processor with 64 cores and 256 GB of RAM. Runtimes of all methods were between 2 – 6h. In total we conducted 450 experiments (5 seeds times 4 + 1 experimental models (CPE, 3 baselines, MCMC references samples) times 9 benchmark tasks times two data set sizes) yielding a total runtime of approximately $1800 * 64 = 115\,200$ CPU hours. We uses the workflow manager `Snakemake` (Köster & Rahmann, 2012) to run all experiments automatically on a Slurm cluster.

D Additional results

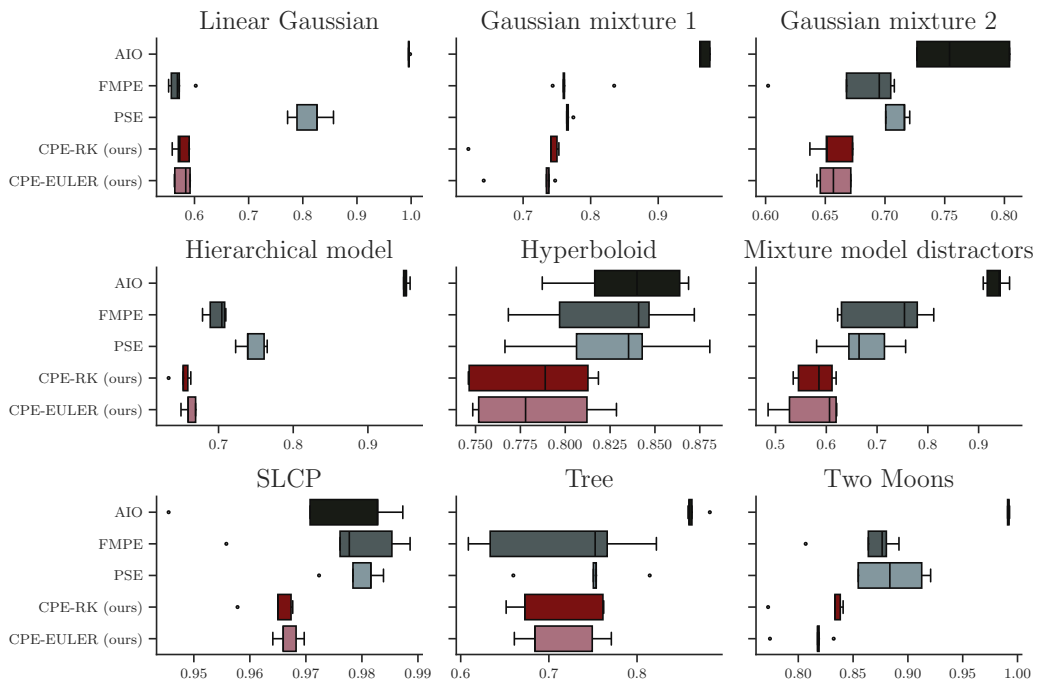


Figure 5: CPE and baseline performance using a C2ST metric (smaller values are better, 0.5 is best) when trained on a data set of size 10 000. CPE-RK denotes the CPE variant that uses a Runge-Kutta 5(4) solver while CPE-Euler uses a 20-step Euler solver.

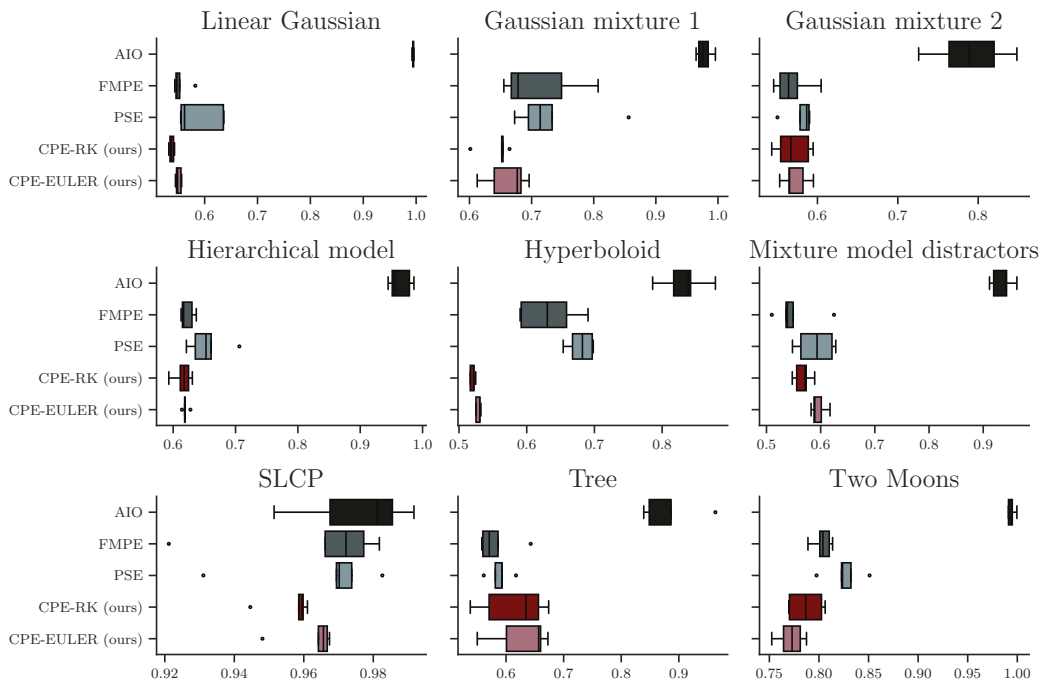


Figure 6: CPE and baseline performance using a C2ST metric (smaller values are better, 0.5 is best) when trained on a data set of size 100 000. CPE-RK denotes the CPE variant that uses a Runge-Kutta 5(4) solver while CPE-Euler uses a 20-step Euler solver.

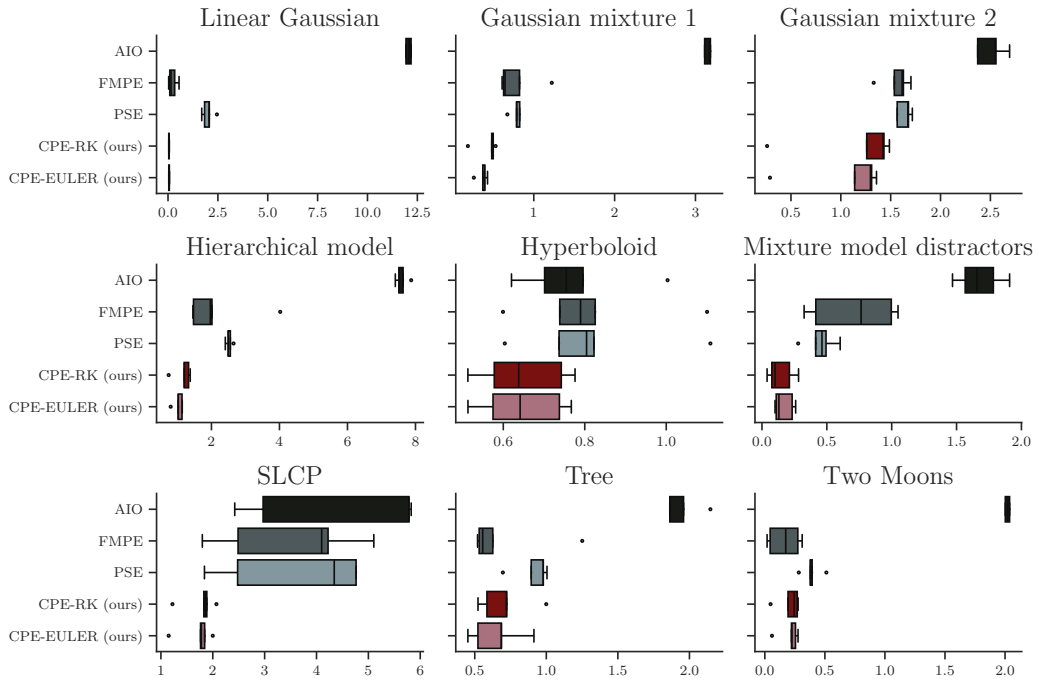


Figure 7: CPE and baseline performance using a H-min metric (smaller values are better) when trained on a data set of size 10 000 (which we include for completeness again). CPE-RK denotes the CPE variant that uses a Runge-Kutta 5(4) solver while CPE-Euler uses a 20-step Euler solver.

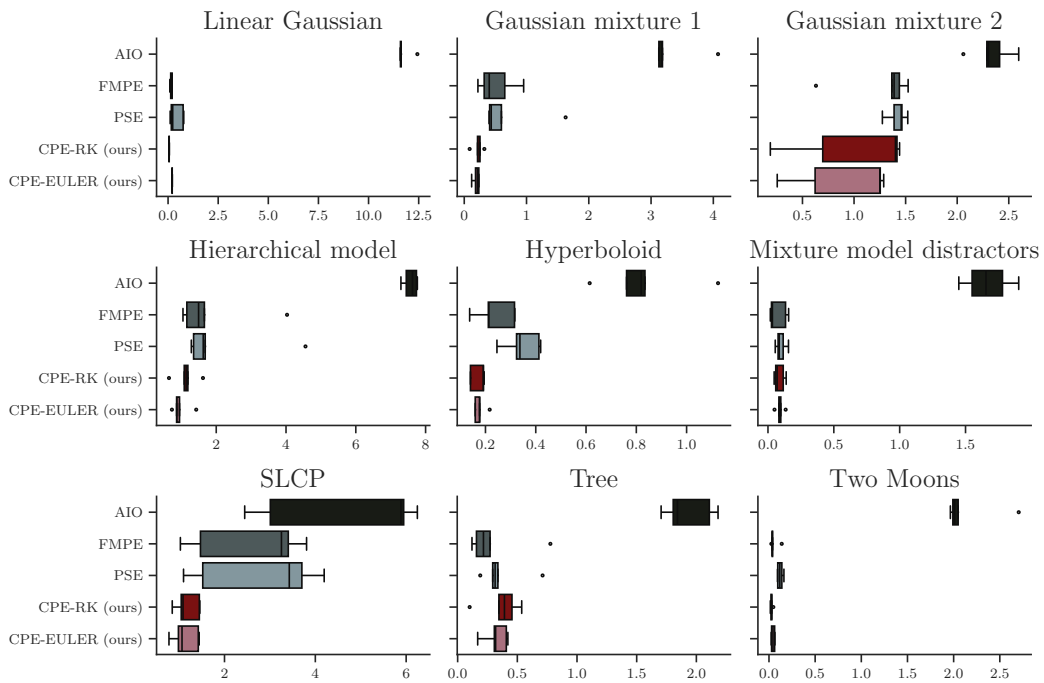


Figure 8: CPE and baseline performance using a H-min metric (smaller values are better) when trained on a data set of size 100 000. CPE-RK denotes the CPE variant that uses a Runge-Kutta 5(4) solver while CPE-Euler uses a 20-step Euler solver.